Pose Measurement of Large Cabin Based on Point Cloud in Multi-robot Assembly

1st Zhe Wang
State Key Laboratory of Management and Control for Complex Systems
Institute of Automation, Chinese Academy of Sciences
Beijing, China
School of Artificial Intelligence
University of Chinese Academy of Sciences
Beijing, China
wangzhe2016@ia.ac.cn

2nd Zhaoyang Liu
State Key Laboratory of Management and Control for Complex Systems
Institute of Automation, Chinese Academy of Sciences
Beijing, China
School of Artificial Intelligence
University of Chinese Academy of Sciences
Beijing, China
liuzhaoyang2017@ia.ac.cn

3rd Junfeng Fan
State Key Laboratory of Management and Control for Complex Systems
Institute of Automation, Chinese Academy of Sciences
Beijing, China
fanjunfeng2014@ia.ac.cn

4th Fengshui Jing*
State Key Laboratory of Management and Control for Complex Systems
Institute of Automation, Chinese Academy of Sciences
Beijing, China
School of Artificial Intelligence
University of Chinese Academy of Sciences
Beijing, China
fengshui.jing@ia.ac.cn

2020 Chinese Automation Congress (CAC) | 978-1-7281-7687-1/20/$31.00 ©2020 IEEE | DOI: 10.1109/CAC51589.2020.9327350

***Abstract*—For multi-robot assembly of two large cabins, the pose measurement of cabin is indispensable. Traditionally, this is achieved by installing targets or markers on the cabins, making the process inefficient. To address this, a pose measurement method based on point cloud which can be readily collected by 3D vision sensor is proposed in this paper. The cylinder model of the cabin is firstly established according to its geometry. The point clouds of cabins are segmented from the point cloud scene using RANSAC model fitting. Then the relative pose between two cabins can be calculated using the segmented point clouds and model coefficients. It is validated in the experiment that the proposed method is accurate and robust for pose measurement of large cabins.**

***Index Terms*—large cabin, point cloud, pose measurement**

I. Introduction

The assembly of large cabins is a fundamental process for the manufacturing of aircraft [1], spacecraft [2], ship [3], etc. Specifically, for the assembly of two separate large cabins, conducting precise initial alignment of two cabins is a pre-requisite, since the poses (including position and orientation) of the cabins need to be aligned properly before joining [4]. Traditionally, in order to align the two cabins, one of the large cabin is hoisted from the ground, while several workers manually adjust its pose, making the whole manufacturing process inefficient and labor intensive. To address this, multi-robot system, which can support the cabin and alter its pose, is adopted in the automatic alignment [5]. For the robotic assembly system, the robot action is based on the feedback of cabin poses, normally given by the measurement of sensor. Therefore, the accurate measurement of cabin pose during the alignment is decisive for the precision and effectiveness of the whole robotic assembly process.

The pose measurement of large cabin in alignment and assembly process is widely studied over the years. Zheng *et al.* [6] proposed a pose fitting method for large cabin assembly. This method adopted SVD point set registration to calculate the pose with the measured key points and the corresponding points on digital models. Then the registration error was optimized using evolutionary computation method, and the final pose of the cabin was thus obtained. Wen *et al.* [7] proposed a position and orientation alignment method for large cabins on Stewart platform. The centers of spherical joints on both moving side and stationary side of Stewart platform were selected as key points. These key points were used to compute the pose of the moving side, along with the cabin fixed on it. Chen *et al.* [8] proposed a position and orientation fitting algorithm during large scale assembly. In this method, considering the structure deformation of the large component, the pose compensation of measured key points on the component was calculated using weighted non-linear optimization. The final pose was computed using SVD registration between model points and measured points with pose compensation. The above mentioned methods realized pose measurement of large cabin during the assembly process.

Research supported by National Natural Science Foundation of China under Grant No.U1813208. *Corresponding author: Fengshui Jing.

Nevertheless, the key points in these methods were manually selected in the CAD model. The results were largely dependent on the selection of the key points by the experts, making the whole process less automatic. Moreover, the sensors in these methods were mainly laser trackers, which generally required targets fixed on the key points of the cabin, thus lowering the efficiency while raising the overall cost.

Comparing to laser tracker, 3D vision sensors, including binocular camera, structured light sensor and TOF camera [9], are able to provide more information with high efficiency for cabin pose measurement. Since 3D vision sensor can capture 3D information of the whole cabin, the key points of the cabin can be automatically determined by feature extraction. In addition, the vision sensors are generally cost-efficient. However, there are also some challenges for the vision measurement. For instance, the surface geometry, texture and color of cabins are generally simple, causing difficulties in feature extraction and the processing afterwards.

There are many researches that involve the pose measurement of large cabin using vision sensors. Zhang *et al.* [10] designed a two-stage iterative algorithm for pose estimation in spacecraft rendezvous and docking, which was similar to cabin alignment. However, in this method, the vision sensor was fixed on the surface of the cabin, and had to be removed manually after the measurement. Wei *et al.* [11] proposed a cabin pose measurement technique based on binocular vision. In this study, visual markers attached on the surface of cabin were leveraged to locate the feature points for pose measurement. The markers required to be placed before the measurement and removed afterwards, inducing inefficiency. Xu *et al.* [12] devised a fast pose registration method for the local area measured by structured light vision sensor in large scale assembly of aircraft. However, this method was not well applicable if the surface curvature of the cabin was identical, since it was based on curvature feature. Hence, the problem of accurate and efficient pose measurement for the large cabins in multi-robot assembly is yet to be fully addressed.

In this paper, a pose measurement method of large cabin based on 3D point cloud in multi-robot assembly is proposed. The point cloud scene containing the cabins and the backgrounds can be captured using a 3D vision sensor from one side of the cabins, with no markers or targets required on the cabins. Then the cabins are segmented from the point cloud and the relative pose between two cabins is computed based on model fitting algorithm, considering that the surface of cabin is texture-less and the geometry of cabin is cylindrical. This method is robust, non-contact and efficient, suitable for the on-site measurement of large cabin during alignment and assembly.

In the remaining part of this paper, the overall system description is presented in Section II. The point cloud segmentation method and pose measurement method are introduced in Section III and Section IV, respectively. In Section V, the experiment results and analyses are provided. Finally, this paper is concluded in Section VI.

II. System Description

A. System Overview

In this research, the cabin assembly system is outlined in Fig. 1. There are two large cabins in this system, which are fixed cabin and movable cabin. The fixed cabin is fastened on a supporting structure with a stable pose. The movable cabin is supported by a supporting structure with four 3-DOF (Degree of Freedom) robots underneath. As the robots move, the pose of the movable cabin is changed accordingly. The objective of this assembly system is to automatically align the end face of movable cabin to the end face of the fixed cabin, so that two cabins can be further joined into one entity via welding or peg-in-hole assembly.

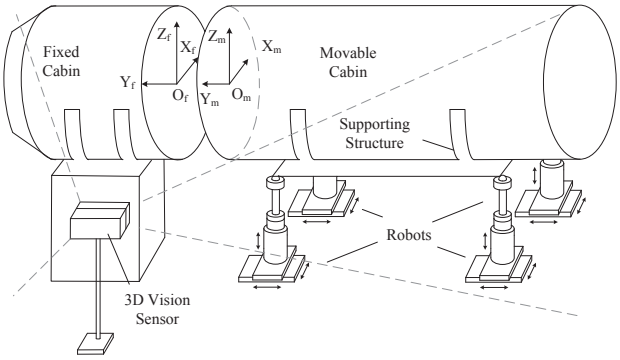

Fig. 1. The outline of cabin assembly system.

To accomplish the alignment, the relative pose between the fixed cabin and the movable cabin needs to be measured. The measurement device is a 3D vision sensor that is able to capture the point cloud of the scene including two cabins in a non-contact fashion. The captured point cloud is a partial view of the scene from one side, upon which the pose is measured.

B. Cylinder Model

Noticing that the large cabins are generally cylindrical, cylinder model is introduced in the model fitting process of the cabin. The cylinder model is illustrated in Fig. 2. Supposing that the cabin is a cylinder whose axis vector is (l, m, n) in Cartesian coordinate and radius is r, all the points (x, y, z) on the cylindrical surface of cabin are subject to the following equation:

$$(x-x_0)^2+(y-y_0)^2+(z-z_0)^2-r^2= \frac{(l(x-x_0)+m(y-y_0)+n(z-z_0))^2}{l^2+m^2+n^2}, \quad (1)$$

where (x_0, y_0, z_0) is a point on the cylindrical axis. Ideally, the points on the cylindrical surface of the cabin point cloud lie on the same model described by (1).

C. Coordinate Definition

As shown in Fig. 1, the coordinate systems of the cabins are composed of fixed cabin coordinate system $\{\mathrm{F}\}$ and movable cabin coordinate system $\{\mathrm{M}\}$. For each system, the origin of the coordinate system is set at the circle center of the cabin

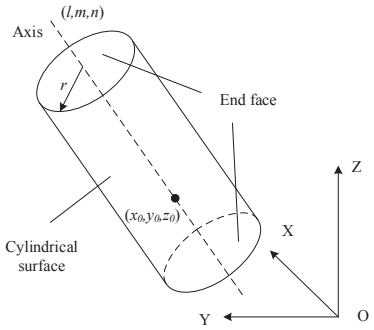

Fig. 2. Definition of cylinder model.

end face. The Y axis is the cylindrical axis whose direction is from the movable cabin to the fixed cabin, the X axis is horizontal on the end face, and the Z axis is derived using right hand rule. The main objective of this research is to obtain the relative pose of the two cabins, which is equivalent to compute the pose between {F} and {M}. Though the 3D point cloud acquired by the vision sensor is defined on the sensor coordinate system {S}, the relative pose between {F} and {M} in the point cloud scene is the same as the actual pose. Therefore, the relative pose measurement is conducted based on the point cloud view given by the sensor.

III. Point Cloud Segmentation

A. Point Cloud Pre-processing

In order to extract the cabin point clouds from the whole scene, point cloud segmentation needs to be conducted. However, the entire point cloud scene captured by the sensor may contain massive amount of points. The segmentation of large amount of points is time consuming, thus lowering the efficiency of this method. Hence, weighted voxel grid filter method is adopted to sample the original point cloud given by the sensor. In this method, the whole point cloud is firstly divided into many voxels with uniform side length. The average 3D position (the center of mass) of all the points inside each voxel is then calculated, and a centroid point is added to the average 3D position to represent the corresponding voxel, replacing the original points inside it. Therefore, the total number of the point cloud is reduced. Compared to voxel grid filter using geometry center of the voxel as centroid, this method is able to better preserve the original curvature of the point cloud.

Moreover, the background of the scene still contains large amount of points, which are redundant during the cabin segmentation. Considering that the background generally contains the floor and the walls, which are mostly large planes, the planar background can be extracted from the scene using RANSAC plane fitting [13], [14]. After the largest plane is fitted, the inliers of the plane are removed from the point cloud and the plane fitting is processed again, until there is no viable plane model detected. Hence the planar background is removed from the point cloud.

B. Cabin Segmentation

To further segment the cylindrical cabins from the scene, RANSAC cylindrical fitting is introduced. Nevertheless, the equation of cylinder has at least six parameters (the three axis vector parameters are correlated). Therefore, six cylindrical surface points are required to fit a cylinder. In RANSAC fitting, the total iteration needed for a reasonably good model is dependant on the sample points for the model computation. Consequently, using six sample points would inevitably increase the total iterations, hence lowering the efficiency.

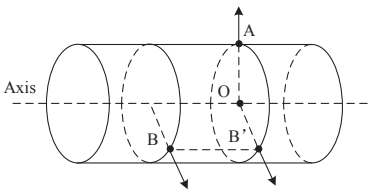

Fig. 3. Cylinder fitting using 2 points with normal vectors.

In this research, the cylinder is instead fitted using sample points with corresponding normal vectors. Thereby, the cylinder model coefficients can be determined using only two points with different normal direction. As shown in Fig. 3, supposing that A and B are the two sampled points with normal vectors, the cylindrical axis can be determined since it is perpendicular to both vectors. Then point B and its normal vector can be projected onto the plane defined by point A and the cylindrical axis. The intersection point O of normal vector of A and B' is the center of cylinder cross section, and the radius can be determined by the length of OA or OB'.

Accordingly, the RANSAC cylinder fitting is conducted subsequently as shown in Algorithm 1. The normal vector of the scene point cloud is estimated using neighbor searching method [14]. In order to prevent that the planar point cloud from being mistakenly identified as cylindrical surface with extremely large radius, a radius limit for the cylinder model is defined in the fitting process.

From the model coefficients, it can be seen that the model is a cylindrical surface with infinite length, so the points from the background or other objects might be falsely included as the model inliers. To address this, point set clustering using Euclidean distance is applied to separate the background segments from the cylindrical cabin, making the cabin a individual entity. Then, the cabin point cloud is extracted and removed from the scene, while the background segments are put back into the scene, in case a part of which belong to another cabin. These procedures are conducted repeatedly, until there is no cylinder model in the scene. Normally after two fitting and clustering procedures, the point clouds of the movable and fixed cabin can be segmented.

IV. Cabin Pose Measurement

A. Cabin Coordinate Determination

From the above fitting process, the cabin cylinder model coefficients $(x_0, y_0, z_0, l, m, n, r)$ in sensor coordinate {S} are obtained. It can be observed in (1) that the cylinder model only

Algorithm 1 RANSAC cylinder fitting

Require: point cloud of the scene
Ensure: the largest cylinder
set desired success probability p_1
estimate cylinder inlier point probability p_2
set threshold d_t and minimum cylinder point sum k_{min}
calculate total iteration $N = log(1-p_1)/log(1-p_2^2)$
initiate point counts $k = k_{min}$
for $t = 1, 2, , N$ **do**
    select 2 random non-collinear points from the cloud
    compute cylinder using the 2 points with normals
    counts the number cnt of points that lie within the threshold distance d_t from the cylinder model
    if $cnt > k_{min}$ and $r_{min} < r < r_{max}$ **then**
        $k = cnt$
        update cylinder coefficients
    end if
end for
if $k > k_{min}$ **then**
    return the cylinder coefficients
else
    return no cylinder model detected
end if

describes a cylindrical surface with no end face, and the axis vector might be directed towards either of the two end faces. Hence the determination of the end faces and the axis direction is necessary.

Firstly, the 3D centroids of the point clouds are computed by averaging 3D positions of the segmented cabin points. A key point on the rim of a end face can be determined by finding the farthest point from the centroid point. Then, the second key point on the rim of the other end face can be determined by searching the farthest point from the first key point.

With the two key points $K_i(x_{ki}, y_{ki}, z_{ki})$, $(i = 1, 2)$ on the end face and cylindrical axis (l, m, n), the corresponding end face plane coefficients can be determined.

$$l(x-x_{ki})+m(y-y_{ki})+n(z-z_{ki}) = 0, \quad i = 1, 2 \tag{2}$$

Then the two circle centers $C_i(x_{ci}, y_{ci}, z_{ci})$, $(i = 1, 2)$ can be calculated by projecting the fitted (x_0, y_0, z_0) on both end faces of a cabin.

$$x_{ci} = \frac{(m^2+n^2)x_0 - l(my_0+nz_0-lx_{ki}-my_{ki}-nz_{ki})}{l^2+m^2+n^2} \tag{3}$$

$$y_{ci} = \frac{(l^2+n^2)y_0 - m(lx_0+nz_0-lx_{ki}-my_{ki}-nz_{ki})}{l^2+m^2+n^2} \tag{4}$$

$$z_{ci} = \frac{(l^2+m^2)z_0 - n(lx_0+my_0-lx_{ki}-my_{ki}-nz_{ki})}{l^2+m^2+n^2} \tag{5}$$

From the fixed and movable cabins, four circle centers are obtained in total. Among them, the two closest center points from the two cabins are designated O_F and O_M, corresponding to the origins of {F} and {M}.

$$O_M = (x_M, y_M, z_M), \quad O_F = (x_F, y_F, z_F) \tag{6}$$

The direction of the Y axis ${}^S\boldsymbol{v}_F$ of {F} and the Y axis ${}^S\boldsymbol{v}_M$ of {M} are defined by finding the cylindrical axis orientation whose angle with the vector ${}^S\boldsymbol{v}_{MF} = \overrightarrow{O_M O_F}$ is smaller.

$${}^S\boldsymbol{v}_{MF} = (x_F - x_M, y_F - y_M, z_F - z_M) \tag{7}$$

$${}^S\boldsymbol{v}_F = \begin{cases} (l_F, m_F, n_F), & (l_F, m_F, n_F)\cdot {}^S\boldsymbol{v}_{MF} > 0, \\ -(l_F, m_F, n_F), & (l_F, m_F, n_F)\cdot {}^S\boldsymbol{v}_{MF} \le 0. \end{cases} \tag{8}$$

$${}^S\boldsymbol{v}_M = \begin{cases} (l_M, m_M, n_M), & (l_M, m_M, n_M)\cdot {}^S\boldsymbol{v}_{MF} > 0, \\ -(l_M, m_M, n_M), & (l_M, m_M, n_M)\cdot {}^S\boldsymbol{v}_{MF} \le 0. \end{cases} \tag{9}$$

Thus, the cabin coordinate {M} and {F} are located in the scene point cloud in the vision sensor coordinate {S}.

B. Pose Computation

As mentioned in Section II, computing the relative pose between two cabins is equivalent to computing the rotation between the Y axis of {F} and the Y axis of {M} and the translation between O_F and O_M.

The rotation can be present by equivalent angle-axis, where unit vector $\boldsymbol{\omega}$ is the rotation axis and θ is the rotation angle around the axis. The computation of the angle-axis is as follows:

$$\theta = \arccos\left(\frac{{}^S\boldsymbol{v}_M \cdot {}^S\boldsymbol{v}_F}{\left|{}^S\boldsymbol{v}_M\right| \left|{}^S\boldsymbol{v}_F\right|}\right) \tag{10}$$

$$\boldsymbol{\omega} = (\omega_x, \omega_y, \omega_z) = \frac{{}^S\boldsymbol{v}_M \times {}^S\boldsymbol{v}_F}{\left|{}^S\boldsymbol{v}_M \times {}^S\boldsymbol{v}_F\right|} \tag{11}$$

The rotation can also be presented by rotation matrix as follows:

$$\boldsymbol{R} = e^{\hat{\boldsymbol{\omega}}\theta} = \boldsymbol{I} + \hat{\boldsymbol{\omega}}\sin\theta + \hat{\boldsymbol{\omega}}^2(1-\cos\theta), \tag{12}$$

where I is identity matrix, and

$$\hat{\boldsymbol{\omega}} = \begin{pmatrix} 0 & -\omega_z & \omega_y \\ \omega_z & 0 & -\omega_x \\ -\omega_y & \omega_x & 0 \end{pmatrix} \tag{13}$$

The relative translation $\boldsymbol{t}$ equals to the vector ${}^S\boldsymbol{v}_{MF}$ in (7). Therefore, the relative pose $(\boldsymbol{R}, \boldsymbol{t})$ is measured.

V. Experiments and Analyses

A. Experimental Setup

In order to verify the effectiveness of the proposed method for large cabins, a simulation experiment was conducted.

In this experiment, the CAD models of the cabins were firstly designed as shown in Fig. 4. The diameter of the aligning side face of the cabin was 2.98m. The cabins were placed in one scene with robots, supporting structures, and the background. To simulate the point cloud scene captured by vision sensor, a virtual sensor was established to render partial point clouds of the CAD models seen from different

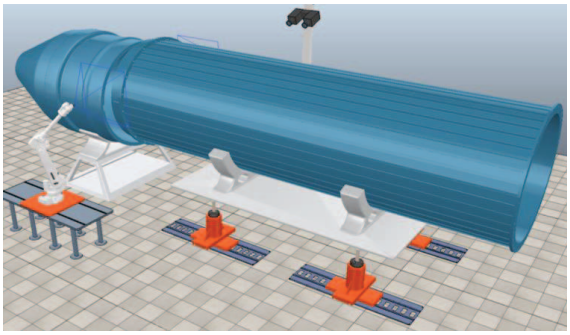

Fig. 4. The CAD models of large cabins.

viewpoints. The partial view taken from one side of the cabins was adopted in this experiment, as it coincided with the above mentioned system configuration. The point cloud scene with 4.75×10^4 data points was obtained as shown in Fig. 5, on which the cabin segmentation and pose measurement experiments were thereafter conducted.

In order to effectively evaluate the pose measurement method, several point cloud scenes containing movable cabin with different ground truth poses were established and rendered. In the initial scene, the pose of movable cabin was aligned with the fixed cabin. Then the movable cabin in the initial pose was rotated plus minus $5°$ and plus minus $10°$, around the X axis and the Z axis of its center coordinate respectively. Thus, totally 9 scenes with different movable cabin poses were constructed.

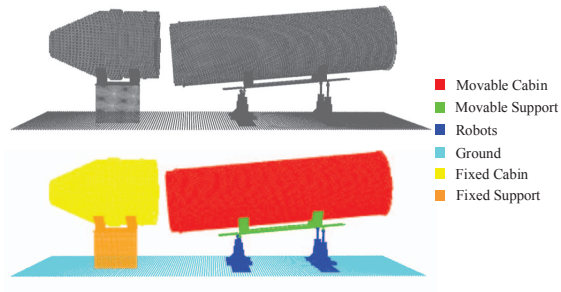

Fig. 5. The rendered point cloud scene: point cloud ensemble (above), point cloud with component annotation (below).

In the experiment of this research, the point cloud processing algorithms introduced above were implemented using C++ language with open source Point Cloud Library (PCL) [15], on a computer with Intel i7-6700 GPU and 8GB RAM.

B. Experiment Results

The fixed and movable cabins were firstly segmented from the point cloud scene. The visualized segmentation result from each step of the segmentation procedure is presented in Fig. 6. And the final segmentation results of two cabins in different poses are shown in Fig. 7. As illustrated by the figures, the proposed segmentation method was able to precisely extract the fixed and movable cabins from the scene.

Based on the segmented cabin point clouds, the coordinates of the cabins were determined and the relative pose was calculated using the proposed method. To demonstrate the performance of the proposed method, ICP registration [16] which was widely applied in pose measurement was adopted in this task as comparison. In this experiment, ICP was used to register the point clouds of fixed and movable cabins previously segmented using the method above, and output the relative pose between the two point clouds.

The measurement errors of the relative pose between the two cabins of 9 scenes are given in Table I and Fig. 8. The rotation errors were represented in Z-Y-X Euler angle measured in degree, and Rot-X, Rot-Y, and Rot-Z represents the rotation error of X, Y, and Z axis, respectively.

Noticing that the cabin was rotationally symmetric along the Y axis, the rotation along the Y axis was relatively trivial in this study, i.e. only the pitch and yaw angles of the cabin were considered important for the pose measurement and alignment. Comparing the rotation error of X and Z axis, our method was more accurate due to the accurate determination of the coordinate of both fixed and movable cabin according to the model fitting result. In contrast, for ICP registration, the fixed and movable cabin was different in size and their point clouds only overlapped partially, resulting in large amount of outliers, thus interfering the performance. In addition, ICP sought to find the largest overlap between point clouds, regardless of difference of viewpoints. Hence, the unnecessary rotation along Y axis was conducted during the ICP registration.

TABLE I
MEASUREMENT ERROR OF THE PROPOSED METHOD AND ICP

Method	Error(°)	Rot-X	Rot-Y	Rot-Z
The proposed method	Mean	0.2130	0.0233	0.3031
	Standard Deviation	0.2224	0.0211	0.2732
ICP registration	Mean	0.6557	7.8228	1.0356
	Standard Deviation	0.5716	6.2030	1.1330

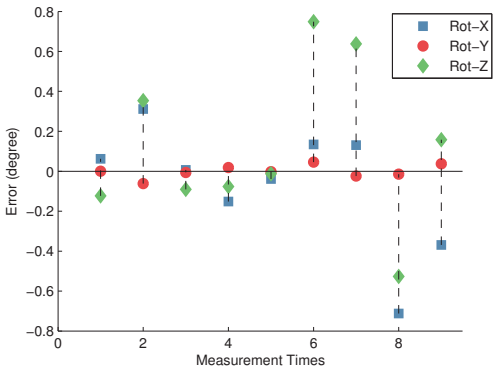

Fig. 8. The measurement error of the proposed method.

VI. Conclusion

In this paper, a pose measurement method of large cabin based on point cloud model fitting for multi-robot assembly is proposed. The major contributions are as follows:

- The proposed method is non-contact and efficient. It only uses point cloud which is easily available with 3D vision

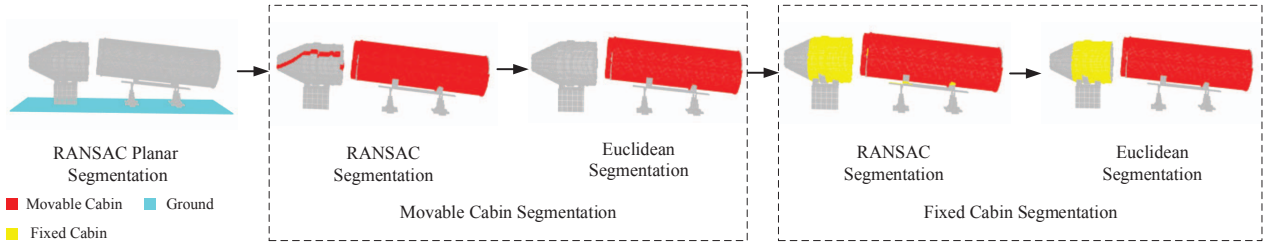

Fig. 6. The visualized segmentation procedure.

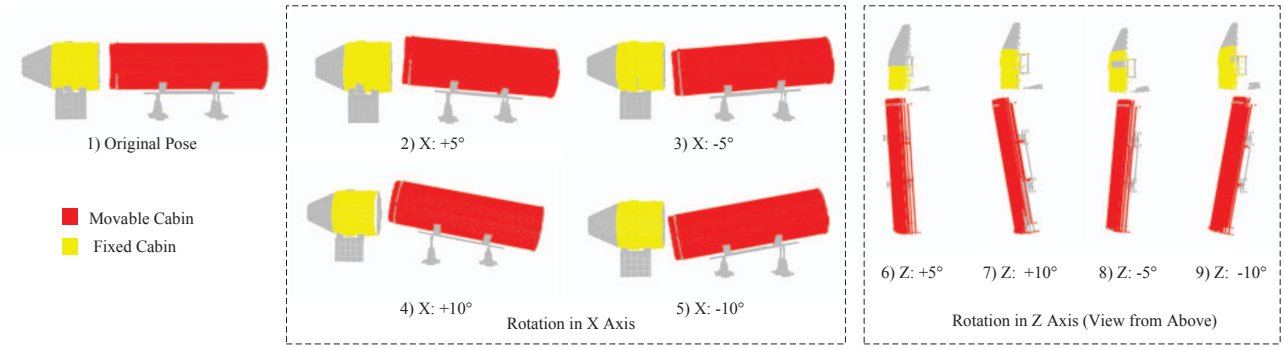

Fig. 7. The segmentation results with 9 different cabin poses.

sensors, without extra requirement for the installation of markers or targets on the cabin for measurement.

- This method is well applicable for the cabins with no distinct texture or curvature features, since the segmentation and pose measurement methods are devised based on cylindrical model fitting of the cabin point cloud.
- As compared to point cloud pose measurement method such as ICP, the proposed method is robust and accurate in the experiment, not interfered by the difference in size of fixed and movable cabins.

In the future work, we will seek to apply this method in on-site measurement of large cabins to facilitate the multi-robot alignment and assembly process.

REFERENCES

[1] P. Lei and L. Zheng, "An automated in-situ alignment approach for finish machining assembly interfaces of large-scale components," *Robotics and Computer-Integrated Manufacturing*, vol. 46, pp. 130–143, 2017.

[2] S. Meng, R. Hu, L. Zhang, and J. Zhao, "Precise robot assembly for large-scale spacecraft components with a multisensor system," in *2017 5th International Conference on Mechanical, Automotive and Materials Engineering (CMAME)*. IEEE, 2017, pp. 254–258.

[3] F.-S. Jing, M. Tan, Z.-G. Hou, Z.-Z. Liang, Y.-K. Wang, M. M. Gupta, and P. N. Nikiforuk, "Kinematic analysis of a flexible six-DOF parallel mechanism," *IEEE Transactions on Systems, Man, and Cybernetics, Part B (Cybernetics)*, vol. 36, no. 2, pp. 379–389, 2006.

[4] Z. Deng, X. Huang, S. Li, and H. Xing, "On-line calibration and uncertainties evaluation of spherical joint positions on large aircraft component for zero-clearance posture alignment," *Robotics and Computer-Integrated Manufacturing*, vol. 56, pp. 38–54, 2019.

[5] F.-S. Jing, M. Tan, Z.-G. Hou, and Y.-K. Wang, "Posture aligning and merging system for boat blocks-realization of coordinated manipulation with a multi-robot system," *Acta Automatica Sinica*, vol. 28, no. 5, pp. 708–714, 2002.

[6] L. Zheng, X. Zhu, R. Liu, Y. Wang, and P. G. Maropoulos, "A novel algorithm of posture best fit based on key characteristics for large components assembly," *Procedia CIRP*, vol. 10, pp. 162–168, 2013.

[7] K. Wen and F. Du, "Framework and implementation of two-stage alignment for large components based on P&O and F/T," *Procedia CIRP*, vol. 56, pp. 73–78, 2016.

[8] Z. Chen, F. Du, and X. Tang, "Position and orientation best-fitting based on deterministic theory during large scale assembly," *Journal of Intelligent Manufacturing*, vol. 29, no. 4, pp. 827–837, 2018.

[9] S. Zennaro, M. Munaro, S. Milani, P. Zanuttigh, A. Bernardi, S. Ghidoni, and E. Menegatti, "Performance evaluation of the 1st and 2nd generation Kinect for multimedia applications," in *2015 IEEE International Conference on Multimedia and Expo (ICME)*. IEEE, 2015, pp. 1–6.

[10] S. Zhang, F. Liu, X. Cao, and L. He, "Monocular vision-based two-stage iterative algorithm for relative position and attitude estimation of docking spacecraft," *Chinese Journal of Aeronautics*, vol. 23, no. 2, pp. 204–210, 2010.

[11] Z.-Z. Wei, Q.-H. Meng, M. Zeng, Y.-B. Liu, Z.-G. Lian, and Z.-Q. Kang, "Stereo vision based cabin's 6-dimensional pose measurement in docking process," in *2018 13th World Congress on Intelligent Control and Automation (WCICA)*. IEEE, 2018, pp. 1279–1283.

[12] J. Xu, R. Chen, H. Chen, S. Zhang, and K. Chen, "Fast registration methodology for fastener assembly of large-scale structure," *IEEE Transactions on Industrial Electronics*, vol. 64, no. 1, pp. 717–726, 2016.

[13] M. A. Fischler and R. C. Bolles, "Random sample consensus: a paradigm for model fitting with applications to image analysis and automated cartography," *Communications of the ACM*, vol. 24, no. 6, pp. 381–395, 1981.

[14] R. B. Rusu, *Semantic 3D object maps for everyday robot manipulation*. Springer, 2013.

[15] R. B. Rusu and S. Cousins, "3D is here: Point Cloud Library (PCL)," in *2011 IEEE International Conference on Robotics and Automation*. IEEE, 2011, pp. 1–4.

[16] P. J. Besl and N. D. McKay, "A method for registration of 3-D shapes," *IEEE Transactions on Pattern Analysis and Machine Intelligence*, vol. 14, no. 2, pp. 239–256, Feb 1992.